THE ASTROPHYSICAL JOURNAL, 501:841–852, 1998 July 10

HUBBLE SPACE TELESCOPE WFPC2 IMAGING OF FS TAURI AND HARO 6-5B[1]

JOHN E. KRIST,[2] KARL R. STAPELFELDT,[3] CHRISTOPHER J. BURROWS,[2,4] GILDA E. BALLESTER,[5] JOHN T. CLARKE,[5]
DAVID CRISP,[3] ROBIN W. EVANS,[3] JOHN S. GALLAGHER III,[6] RICHARD E. GRIFFITHS,[7] J. JEFF HESTER,[8]
JOHN G. HOESSEL,[6] JON A. HOLTZMAN,[9] JEREMY R. MOULD,[10] PAUL A. SCOWEN,[8]
JOHN T. TRAUGER,[3] ALAN M. WATSON,[11] AND JAMES A. WESTPHAL[12]
Received 1997 December 18; accepted 1998 February 16

ABSTRACT

We have observed the field of FS Tauri (Haro 6-5) with the Wide Field Planetary Camera 2 on the *Hubble Space Telescope*. Centered on Haro 6-5B and adjacent to the nebulous binary system of FS Tauri A there is an extended complex of reflection nebulosity that includes a diffuse, hourglass-shaped structure. H6-5B, the source of a bipolar jet, is not directly visible but appears to illuminate a compact, bipolar nebula which we assume to be a protostellar disk similar to HH 30. The bipolar jet appears twisted, which explains the unusually broad width measured in ground-based images. We present the first resolved photometry of the FS Tau A components at visual wavelengths. The fluxes of the fainter, eastern component are well matched by a 3360 K blackbody with an extinction of $A_V = 8$. For the western star, however, any reasonable, reddened blackbody energy distribution underestimates the K-band photometry by over 2 mag. This may indicate errors in the infrared photometry or errors in our visible measurements due to bright reflection nebulosity very close to the star. The binary was separated by $0\farcs239 \pm 0\farcs005$ at a position angle of $84° \pm 1\fdg5$ on 1996 January 25. There is no nebulosity around FS Tau A at the orientation suggested for a disk based on previous, ground-based polarization measurements.

Subject headings: binaries: visual — circumstellar matter — ISM: jets and outflows — stars: individual (FS Tauri, Haro 6-5B)

1. INTRODUCTION

The Wide Field and Planetary Camera 2 (WFPC2) Investigation Definition Team has been using the *Hubble Space Telescope* (*HST*) to image circumstellar material around young stellar objects. The selection criteria for the program are a high millimeter flux (suggestive of a circumstellar disk) and/or a high optical polarization (which indicates surrounding reflection nebulosity). Results have been obtained for HH 30 (Burrows et al. 1996), HL Tauri (Stapelfeldt et al. 1995), XZ Tauri (Krist et al. 1997), T Tauri (Stapelfeldt et al. 1998a), GM Aurigae (Stapelfeldt et al. 1998b), DG Tauri (Burrows et al. 1998), GG Tauri (Burrows et al. 1998), and Coku Tau/1 and Schwartz 102 (Stapelfeldt et al. 1997). The field of FS Tauri contains two objects that also meet these criteria.

FS Tauri A (Haro 6-5, HBC 383) is located in the Taurus star-forming region, 140 pc away (Elias 1978). Lunar occultation observations revealed it to be a binary system separated by about $0\farcs25$ (Chen et al. 1990; Simon et al. 1992). A composite M1 spectral type was assigned to the system by Cohen & Kuhi (1979). FS Tau A is one of the more highly polarized ($\sim 10\%$) T Tauri stars (Gledhill & Scarrott 1989; hereafter, GS89), indicating a possible circumstellar disk.

About $20''$ to the west of FS Tau A is the young star Haro 6-5B (FS Tauri B, HBC 381). It was discovered by Mundt et al. (1984), who showed that it was associated with a Herbig-Haro (HH) jet. It is situated at the apex of a cone of reflection nebulosity that extends to the northeast. The bipolar jet at position angle (P.A.) = 54° is designated HH 157. It extends at least $6'$ to the northeast and $38''$ to the southwest, as seen from ground-based telescopes. The northeast jet is blueshifted and has radial velocities of -30 to -70 km s^{-1}, while the redshifted southwest jet has velocities of $+60$ to $+80$ km s^{-1} (Mundt, Brugel, & Bührke 1987; hereafter, MBB87). For typical flow speeds of 300 km s^{-1}, these radial velocities suggest that the jets are directed roughly 13° from the plane of the sky. The jet appears to narrow with distance in ground-based images (Mundt, Ray, & Raga 1991; hereafter, MRR91). H6-5B also has a high optical polarization ($\sim 9\%$) oriented at P.A. = $147° \pm 8°$ (Gledhill, Warren-Smith, & Scarrott 1986). A compact, dense clump of molecular gas is seen at the position of Haro 6-5B (Dutrey et al. 1996), and strong 1.3 mm continuum emission has been detected for the source (Reipurth et al. 1993). Recent

[1] Based on observations with the NASA/ESA *Hubble Space Telescope*.

[2] Space Telescope Science Institute, 3700 San Martin Drive, Baltimore, MD 21218; krist@stsci.edu.
[3] MS 183-900 Jet Propulsion Laboratory, Pasadena, CA 91109.
[4] Astrophysics Division, Space Science Department, European Space Agency.
[5] Department of Atmospheric, Oceanic, and Space Sciences, University of Michigan, 2455 Hayward, Ann Arbor, MI 48109.
[6] Department of Astronomy, University of Wisconsin, 475 North Charter Street, Madison, WI 53706.
[7] Department of Physics, Carnegie-Mellon University, Wean Hall, 5000 Forbes Avenue, Pittsburgh, PA 15213.
[8] Department of Physics and Astronomy, Arizona State University, Tyler Mall, Tempe, AZ 85287.
[9] Department of Astronomy, New Mexico State University, Box 30001, Department 4500, Las Cruces, NM 88003.
[10] Mount Stromlo and Siding Springs Observatories, Australian National University, Weston Creek Post Office, ACT 2611 Australia.
[11] Instituto de Astronomi'a UNAM, 58090 Morelia, Michoacan, Mexico.
[12] Division of Geological and Planetary Sciences, MS 170-25 Caltech, Pasadena, CA 91125.

imaging and spectroscopy of the jet and surrounding nebulosity has been reported by Eislöffel & Mundt (1998; hereafter, EM98).

2. OBSERVATIONS

The FS Tau field was observed using the Wide Field and Planetary Camera 2 (WFPC2) on the *HST* on 1996 January 25 (*HST* Program 6223). Two 400 s exposures in filter F675W (WFPC2 *R* band) were taken with the field centered on Wide Field Camera 3 (WF3) (0.″1 pixel^{-1}) at a gain of $7e^-$ DN^{-1}. The F675W filter contains the most significant HH object emission lines, and these images were intended to detect low surface brightness jet emission. The field was then moved to the center of the Planetary Camera (PC) (0.″0455 pixel^{-1}), where two exposures of 350 s each (gain = 7) and one of 30 s (gain = 14) were taken in F814W (WFPC2 *I* band). Another two exposures of 100 s each (gain = 14) were taken in F555W (WFPC2 *V* band) at the same location. The two stars constituting FS Tau A were saturated in the F675W and long F814W images.

The images were calibrated using the standard *HST* data pipeline. Duplicate exposures were added together, rejecting cosmic rays. Comparisons between the PC images and the lower resolution WF3 images were done using data corrected for geometrical distortion.

3. RESULTS

3.1. *Overview*

The WFPC2 images reveal complex reflection nebulosity throughout the FS Tau field. Most of this nebulosity appears in both the *R*-band (Fig. 1) and the *I*-band images with similar morphology, which indicates that it is dominated by reflected light from FS Tau A and H6-5B. Much of the nebulosity is underexposed in the *V* image. The *R*-band image clearly shows the bipolar jet from H6-5B aligned along the northeast-southwest direction. H6-5B is obscured from direct view by what appears to be a circumstellar disk (Fig. 2). A large hourglass-shaped structure of reflection nebulosity centered on H6-5B extends out to about 1′ on each side of the jet source, and its symmetry axis is aligned along the jet axis (Fig. 3). A region of dark nebulosity appears to fill the interior of the northeast lobe of the hourglass. A bright, cone-shaped reflection nebula (called R1 by MBB87) extends nearly 8″ to the northeast of H6-5B. An arc of nebulosity (called R2) lies within the southwest lobe of the hourglass, 9″ from H6-5B. FS Tau A is surrounded by complex nebulosity, and it appears to illuminate the southwest edge of the dark nebula. Contour plots of the region are shown in Figure 4.

3.2. *FS Tau A (Haro 6-5)*

The F555W (*V*-band) and the 30 s F814W (*I*-band) images show the brightest portions of the reflection nebula around FS Tau A. In the F555W frame, the nebulosity appears confined to a cone extending to the southeast at a position angle of 132°, with an opening angle of about 80° and an overall length of about 6″. Material can be traced to within 0.″2 of the stars, where the diffraction structures of the stellar point spread functions (PSFs) begin to dominate. The western component (hereafter FS Tau W) is clearly visible, but the eastern, fainter companion (FS Tau E) is barely above the level of the surrounding nebulosity. The F814W image clearly resolves the two stars. FS Tau E noticeably increases in brightness relative to FS Tau W in comparison to the F555W frame. The nebulosity on the east side of the system likewise brightens. The stars are unsaturated in both images.

In the F675W (*R*-band) and long F814W images, more nebulosity becomes apparent (Fig. 2). FS Tau A appears to illuminate the straight edge of a dark nebula ~5″ north of the system, forming a 15″ long streak oriented in the northeast-southwest direction at P.A. = 71°. Light from both FS Tau A and H6-5B seems to illuminate this edge, as was noticed by GS89. A small arc is seen 0.″9 to the northwest of the system. The nebulosity to the northwest near the stars is filamentary. There is no indication of emission structures associated with FS Tau A.

For both the F555W and short F814W images, the two stars were simultaneously fit with theoretical PSFs produced by the Tiny Tim software (Krist 1996), using the methods described by Krist et al. (1997). Photometry, separations, and position angles were derived from these fits. The positions are accurate to approximately ± 0.05 pixels, and the position angle is accurate to within $\pm 1.^\circ 3$. The instrumental fluxes were translated to standard *V* and *I* magnitudes using synthetic photometry software and assuming an M1 spectral type source. The total estimated flux error from the PSF fitting and filter conversion is ± 0.1 mag (mostly due to conversion uncertainties). The F555W flux for FS Tau E should be considered an upper limit owing to possible contributions from the surrounding nebulosity. The measurements are given in Table 1 along with photometry from synthetic apertures centered on the system. The F814W astrometry is included, with the position angle measured from north to east along a line from the brighter star (FS Tau W) to the fainter one. In the F675W image, the stars are saturated and blend together because of the lower resolution of the Wide Field Camera, so no *R*-band photometry is provided.

The photometry shows that FS Tau E is redder than FS Tau W. In the *V* band, the west/east flux ratio is 18.5, and in *I* it is 7.3. Using lunar occulation observations, Simon et al. (1992) measured $K = 7.4$ for FS Tau W and $K = 10.08$ (1989 March) to 9.7 (1989 September) for FS Tau E, which gives flux ratios of 11.9 and 8.2, respectively. It appears that FS Tau E remains less luminous at all wavelengths compared to FS Tau W.

The synthetic aperture fluxes are consistent with those of Vrba, Rydgren, & Zak (1985; hereafter, VRZ85). The aperture photometry values are about 0.5 mag more blue than our combined stellar measurements owing to contamination from the surrounding reflection nebulosity.

Our separation and position angle are somewhat different than those of Simon et al. (1992). They derived a separation of $0.''265 \pm 0.''005$ at P.A. = $60^\circ \pm 5^\circ$ using data from 1989 March and September (their position angle was measured eastward from north from the brighter star to the fainter one, as was ours). If FS Tau A consisted of 1 and 0.5 $M_\odot$ stars and a separation of 0.″3 (42 AU) represented the semimajor axis of the orbit, then the system would have an orbital timescale on the order of 200 yr. A circular orbit would show a position angle change of about 11° during the 6 yr between our and their observations and may explain most of the differences in separation and alignment. However, a comparison of binaries common to the speckle observations of Ghez, Neugebauer, & Matthews (1993) and lunar occulation observations of Simon et al. (1992) show

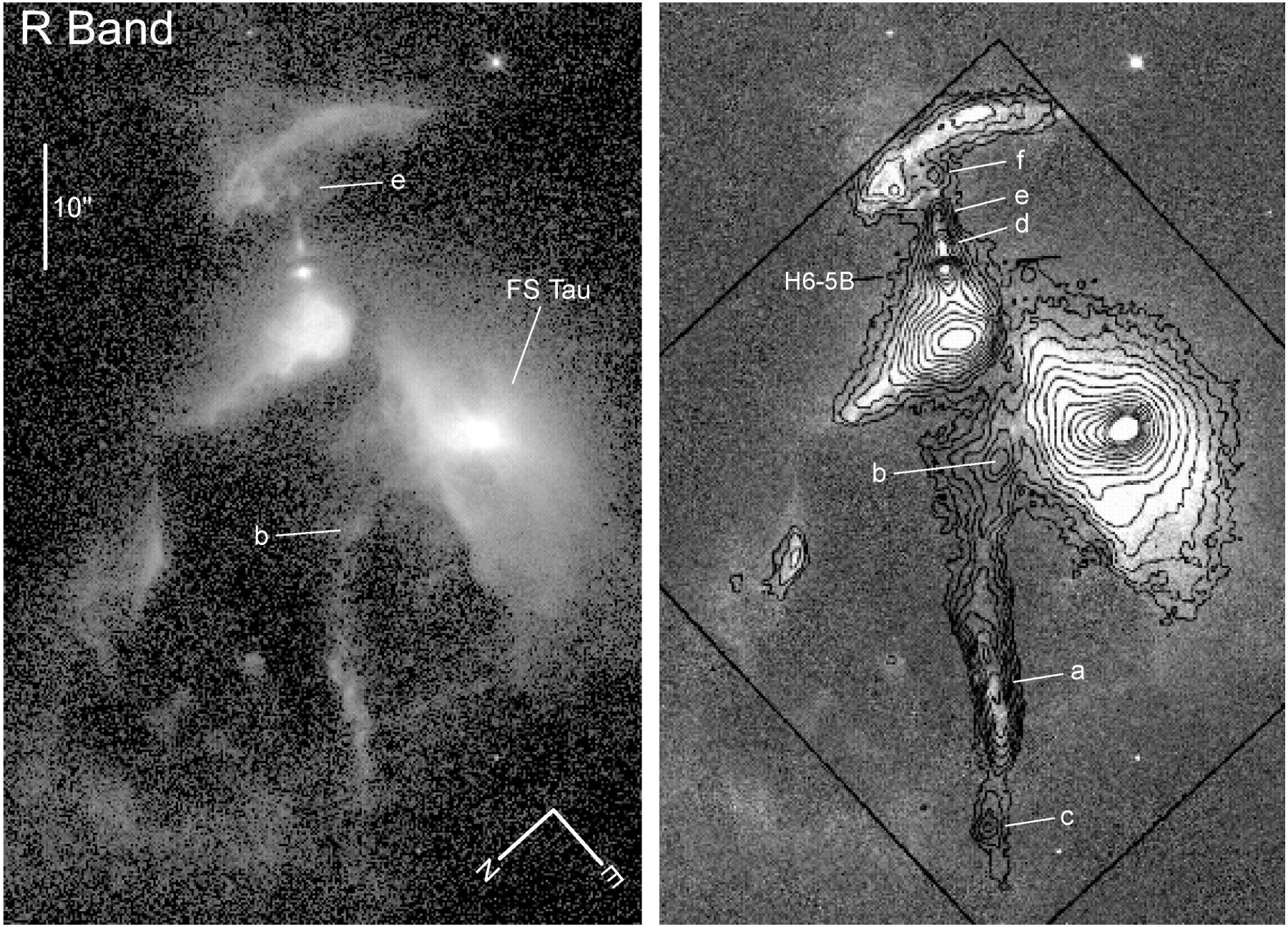

FIG. 1.—*Left:* WFPC2 F675W (*R*-band) image of the field of FS Tauri and Haro 6-5B, logarithmically scaled; *right:* WFPC2 F675W image overlaid with the Hα − *I* contour plot from Mundt et al. (1991) (used with permission). The ratio between contours is $2^{1/2}$. Their knot identification scheme is used.

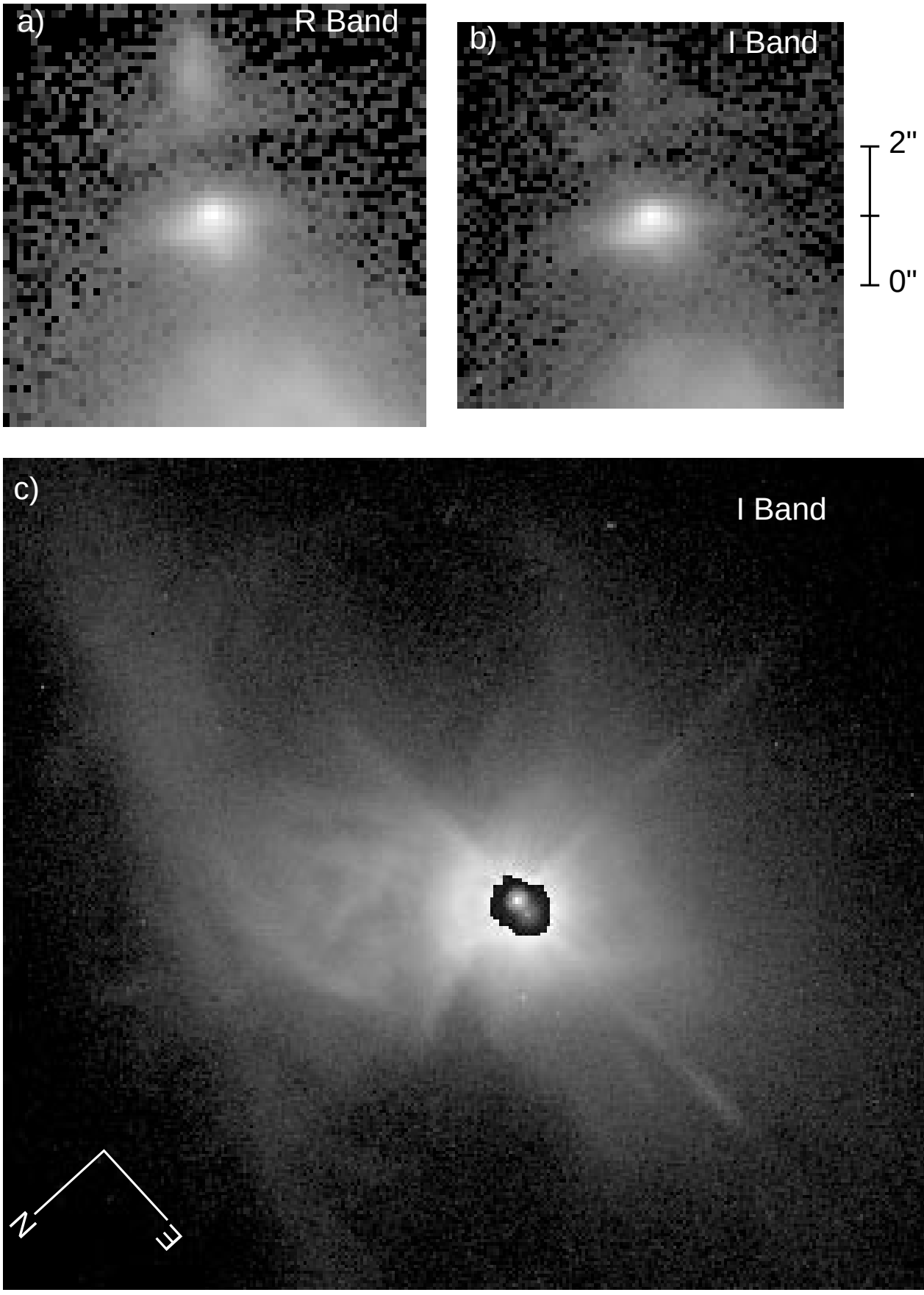

FIG. 2.—Haro 6-5B in (*a*) F675W (*R* band) and (*b*) F814W (*I* band); (*c*) FS Tauri A in the long exposure F814W (*I* band), with the short F814W exposure replacing the central pixels, scaled for contrast. All images are logarithmically scaled.

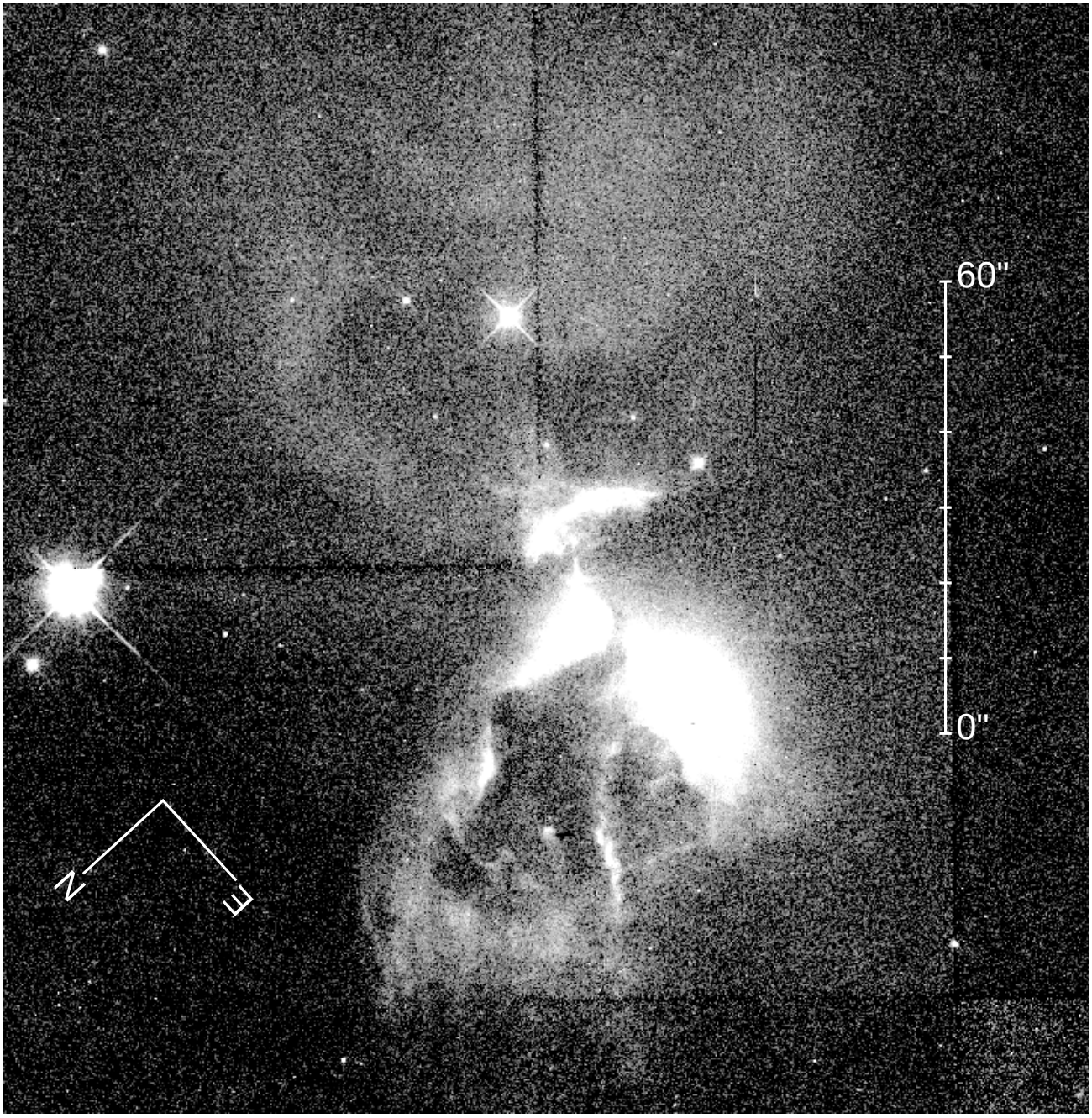

FIG. 3.—Merged F675W (*R*-band) and F814W (*I*-band) images showing the large-scale features in the FS Tauri field, including the hourglass-shaped reflection nebulosity centered on Haro 6-5B. The F675W image occupies the lower right-hand corner of the frame and shows the jet. Detector boundaries are visible as horizontal and vertical dark lines. The image has been logarithmically stretched.

TABLE 1

PHOTOMETRY OF FS TAU BINARY

Parameter	*V*	*I*	*V* − *I*
West point source	17.13	13.99	3.14
East point source.....	20.43	16.27	4.16
Combined point sources.....	17.08	13.86	3.22
Aperture 2″ radius	15.98	13.15	2.83
Aperture 3″ radius	15.78	13.03	2.75
Aperture 4″ radius	15.65	12.95	2.70

NOTE.—Measured binary separation is 0.″2387 ± 0.″005 (33 AU) at P.A. 84.38° ± 1.°5.

significant differences on the order of tens of degrees in the position angles for some of the objects (although the flux values are comparable). We therefore do not place any significance on the positional differences between our measurements and the earlier measurements.

3.3. *Haro 6-5B (FS Tau B)*

The F675W and long F814W images reveal no directly visible star in the H6-5B system. Instead, a compact, bipolar nebula is seen at the stellar position and is distinctly separated from the bright R1 nebula nearby. The circum-

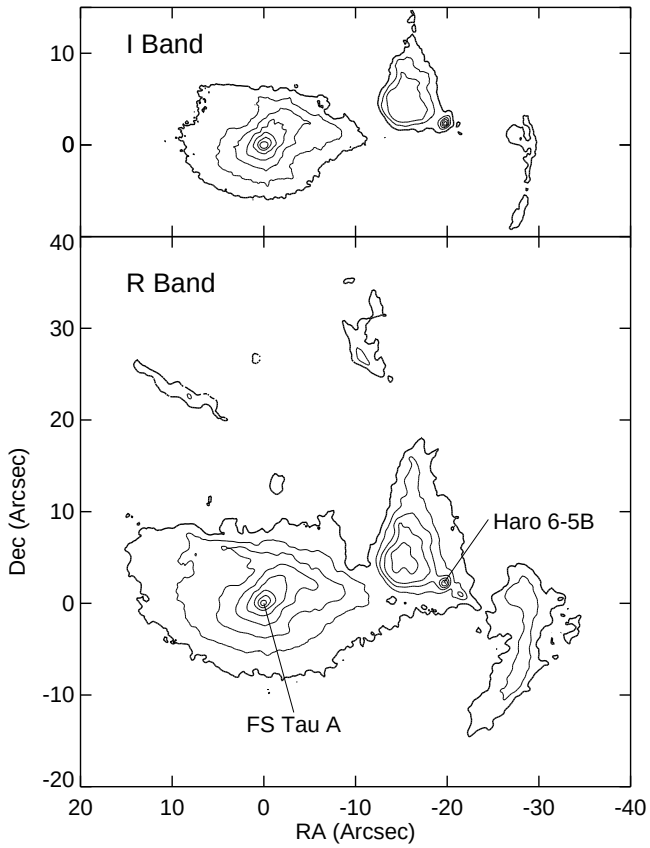

FIG. 4.—Surface brightness contour plots of FS Tauri/Haro 6-5B in F675W (*R* band) and F814W (*I* band). The faintest contour in the *R* band is 23 mag arcsec^{-2} and 21 mag arcsec^{-2} in the *I* band. Contours are spaced by 1 mag arcsec^{-2}.

stellar nebula consists of two curving and parallel arcs of reflection nebulosity that are concave toward the northeast and separated by 1″. Between these nebulae, a dark lane is seen. The circumstellar nebula has a striking overall resemblance to the morphology of the HH 30 system (Burrows et al. 1996). We identify the dark lane as a circumstellar disk seen close to edge-on. The two small reflection nebulosities are presumably the upper and lower surfaces of an optically thick disk that is centrally illuminated and seen in scattered light from the star. The apparent disk diameter is ∼3.″4 (476 AU).

The compact bipolar nebula has integrated fluxes of $V = 20.0$, $R = 19.5$, and $I = 18.2$. Note that the *R*-band flux may include some contamination from the jet, and the *V*-band flux includes only the brightest portion of the northeast component. The northeast component is much brighter than the southwest one by a factor of 34 in integrated flux or 20 in mean surface brightness. Such an asymmetry is expected for reflected light from an inclined disk, where the disk itself obscures view of reflected light on the side tilted away from the observer. The disk plane orientation is at P.A. = 144° ± 3°, which is almost exactly perpendicular to the collimated jet. The bright northeast component of the circumstellar nebula lies on the same side of the dust lane as the blueshifted optical jet, as required in this scenario. The northeast component has a bright central concentration of light. It is asymmetrical, with the northern half brighter than the southern half. A somewhat similar asymmetry was seen in the *HST* images of the HH 30 disk. The southwest component is just above the noise in the F675W and long F814W images, and only the brightest portion of the northeast component is seen in the F555W and short F814W exposures.

3.4. *The Jet*

Since no narrowband images were taken with the *HST*, emission features were differentiated from reflection by comparing the F675W and long F814W exposures. The F675W filter bandpass contains the [O I], Hα, [N II], and [S II] lines that dominate emission in HH object jets. The F814W filter contains weaker lines such as [Fe II], so jet features are expected to be brighter in F675W relative to the reflection nebulosity than in F814W. This is demonstrated in the $R-I$ image in Figure 5.

The base of the northeast jet is indistinctly seen against the background of bright reflected light near the source. A small knob of the jet can be seen just beyond the disk nebulosity, and then the jet disappears before entering the conical R1 nebula. It seems to reappear as a knot 19″ from H6-5B at a position offset about 3″ southeast from the large-scale jet axis. This part of the jet appears to correspond to knot B as identified by MRR91 if significant proper motions are allowed (377 km s^{-1}). Between this position and the R1 nebula there is some diffuse nebulosity, which from its comparable brightness in *R* and *I* bands seems to be reflected light from FS Tau A. The jet continues for 11.″5 along P.A. = 40°. In this region the outflow is poorly defined, although it appears to follow a helical pattern. At 32″ from H6-5B, it suddenly becomes brighter and turns to P.A. = 64°. For the next 10″ it remains bright, with the helical pattern becoming better defined. This length of the jet corresponds to knot A in MRR91. After this bright section, the jet decreases in intensity and turns to P.A. = 52°. We were unable to definitively identify knot C, since it probably lies within the "bridge" of reflection nebulosity at the end of the northeast hourglass lobe (the F814W image does not cover this area). A large and diffuse knot can be identified 63″ from H6-5B (near the bottom of Fig. 3) and corresponds to the last, unlabeled knot in the northeast jet visible in the CCD image of MRR91 and labeled as knot I by EM98. Another, still fainter and diffuse patch can be identified 2′ northeast of the star at P.A. = 57° in Wide Field Camera 4 (not shown in the figures) that is extended along the direction of the outflow and that may be part of the jet. This corresponds to the bow-shaped shock of knot L of EM98. Its surface brightness is approximately $R = 25$ mag arcsec^{-2}.

The jet to the southwest contains the brightest knots and is well collimated. In the raw *R*-band image, it extends from the southwest edge of the disk as a series of knots and ends 5.″4 later at P.A. = 233°, before reaching the arc-shaped reflection nebula R2. In the $R-I$ image shown in Figure 5, it appears to extend into R2, 10″ from H6-5B. MRR91 detected two knots 23″ and 38″ from the star, but our F675W image ends at 22″. The jet is comprised of at least six knots that decrease in intensity with distance from H6-5B. MRR91 saw three knots in the southwest jet within 9″ of the source in their 1987 data. Our higher resolution images show that the two knots closest to the source star in their data (knots D and E) each splits into two knots.

A bright, compact nebula is seen in the *R*-band frame, located 32.″5 northeast of H6-5B and 7″ northwest of the jet, and is identified as c_5 by EM98. It is outside of the F814W

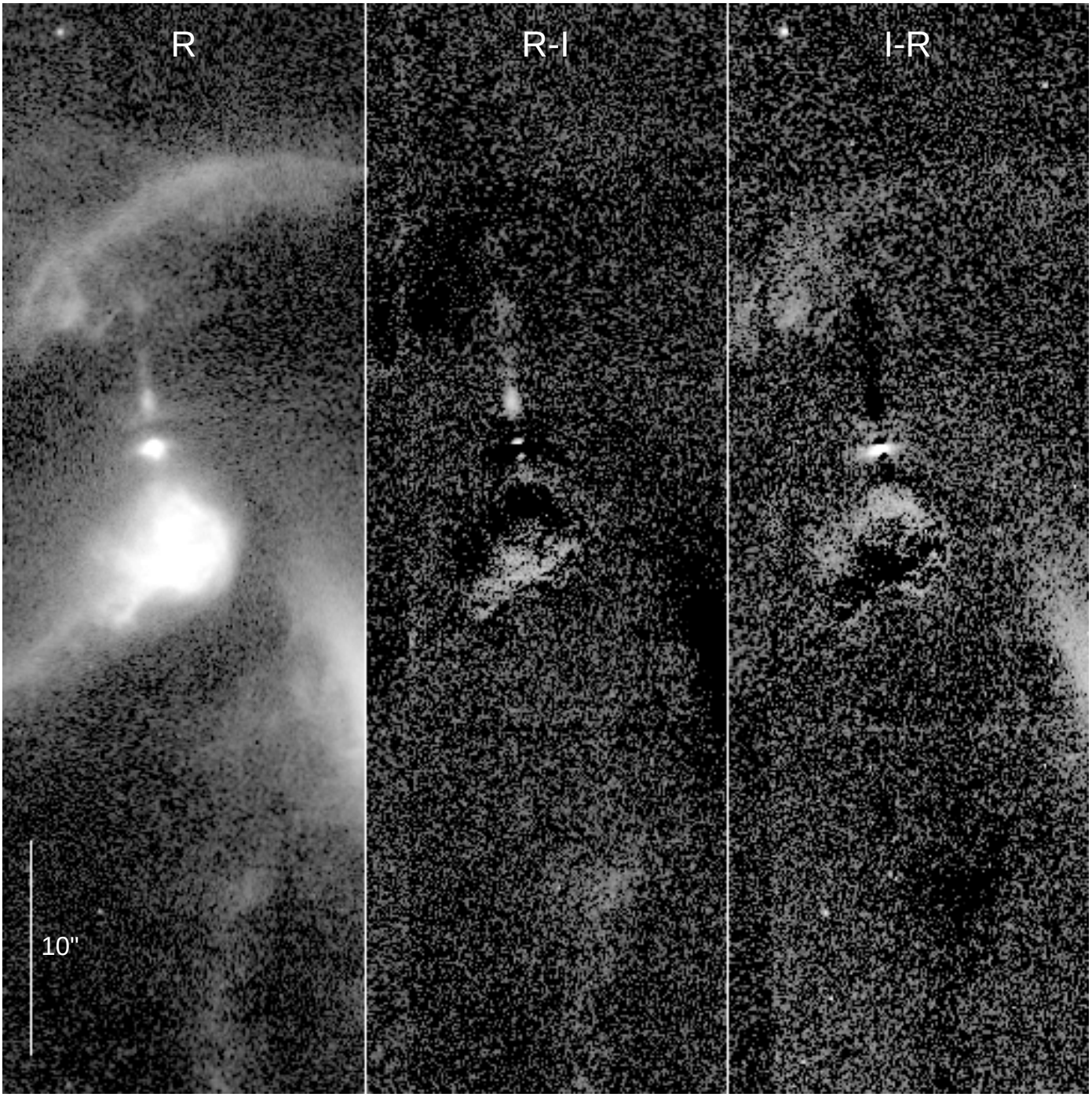

FIG. 5.—*R*-band, $R-I$, and $I-R$ images of the Haro 6-5B disk and jet. The images are logarithmically stretched.

image. It appears to be stationary since it has the same location in the images of MRR91, so we assume that it is reflection nebulosity.

Knot widths can be measured in only a few places due to the generally poor definition of the jet and its faintness. On the southwest side, 300 AU from the peak in the disk, the FWHM is 56 AU (0.″4). At other locations in the jet, the FWHM varies between 56 and 70 AU.

Figure 1 shows our *R*-band image with the Hα contour map of MRR91 overlaid. The image and map were aligned by matching the positions of H6-5B, nebula R2, and other reflection nebulae common to both. From this overlay, the positions of the knots were measured by eye, which are presented in Table 2. The knot labeling scheme of MRR91 is used. Approximate proper motions can be derived for the jet knots if it is assumed that the combined jet emission seen in the *R* bandpass closely follows the emission morphology seen in Hα. Our proper motion measurements agree with those of EM98, including the high velocity of knot B and excepting knot C, which we could not differentiate from reflection nebulosity.

3.5. *Reflection Nebulosity*

H6-5B lies near the apex of the cone-shaped reflection nebula R1 that extends nearly 8″ northeast from the disk. The R1 cone has an opening angle of about 75° and is

TABLE 2

JET KNOT POSITIONS AND PROPER MOTIONS

Knot	1987	1997	Motion	Velocity
A	−34.3	...	<4	<300
B	−16.1	−21.0	5.1	377
C	−45.7	?		<150
D	1.8	3.4	1.6	118
E	4.3	6.4	2.1	155
F	7.7	10.6	2.9	215

NOTE.—Distances and motions are expressed in arcseconds from Haro 6-5B. Negative distances refer to blueshifted knots. Velocities are estimated to be accurate to ± 30 km s^{-1}.

oriented along the jet axis. There is a 1″ gap between the northeast side of the circumstellar nebula and the apex of the cone. The interior of the R1 nebula is mottled, and the intensity falls off toward the edges. This nebula was noted by Mundat et al. (1984), who classified it by both imaging and spectroscopy as reflective. Likewise, Cohen & Fuller (1985) identified continuum flux from it. The spectra of MBB87 showed a significant Hα line, which is likely due to the T Tauri-like spectrum of H6-5B. Its average surface brightnesses in our images are $I = 18.6$ mag arcsec^{-2} and $R = 19.4$ mag arcsec^{-2}. Based on the polarization vectors of the surrounding nebulosity, GS89 concluded that an object within this nebula, which they called Haro 6-5C, was the primary source of illumination for the region. The *HST* images show no indication of any object within the R1 nebula.

Nine arcseconds to the southwest of the disk is a 20″ long arc of filamentary reflection nebulosity, identified as R2 in MBB87. The arc is not centered on H6-5B or on any visible object in the field. Its average surface brightnesses are $I = 21.2$ mag arcsec^{-2} and $R = 22.0$ mag arcsec^{-2}.

At arcminute scales, the surrounding reflection nebulosity forms an hourglass-shaped structure centered on H6-5B and aligned along the jet axis. The opening angle of this hourglass is $\sim 94°$, and lines drawn along its limbs intersect at H6-5B. The northeast lobe has been mentioned by previous observers and the southwest lobe only by EM98. The southwest lobe is seen only in our long F814W image and is outside of the F675W field. Within the northeast lobe, there appears to be a dark nebula from which a projection creates a dark lane in the southern edge of the hourglass, separating FS Tau A and H6-5B. Both ends of the hourglass appear closed by reflective arcs. The light spanning the end of the northeast lobe forms what GS89 described as a "bridge." The hourglass is fairly symmetrical on its northern half, but the southern half is distorted by dark nebulosity and reflected light from FS Tau A.

The limbs of the northeast lobe have an average surface brightness of $I = 22.8$ mag arcsec^{-2} compared to the fainter southwest lobe, where $I = 23.6$ mag arcsec^{-2}. The northeast lobe is probably brighter due to the greater density of reflecting material provided by the dark nebula. This lobe is also presumably tilted toward us by the same amount as the disk and jet.

Figure 5 shows $R-I$ and $I-R$ images of the Haro 6-5B disk and jet. The exposures were normalized so that most of the R1 cone nebula would be subtracted in $I-R$. The jet is well separated from the reflection nebulosity in the $R-I$ frame, and the disk is obvious in $I-R$ due to reddening of starlight by the disk itself. The central concentration of light appears to be bluer than the rest of the disk, probably due to the lower extinction, more direct path of light from the source. These images show that the edges of the R1 nebula are redder than its interior.

3.6. *Disk Modeling*

In Burrows et al. (1996), the structure of the HH 30 disk was derived by iteratively generating simulated images based on three-dimensional, single-scattering models of the dust distribution and comparing them to the observed disk. Using the same form for the density distribution and model-

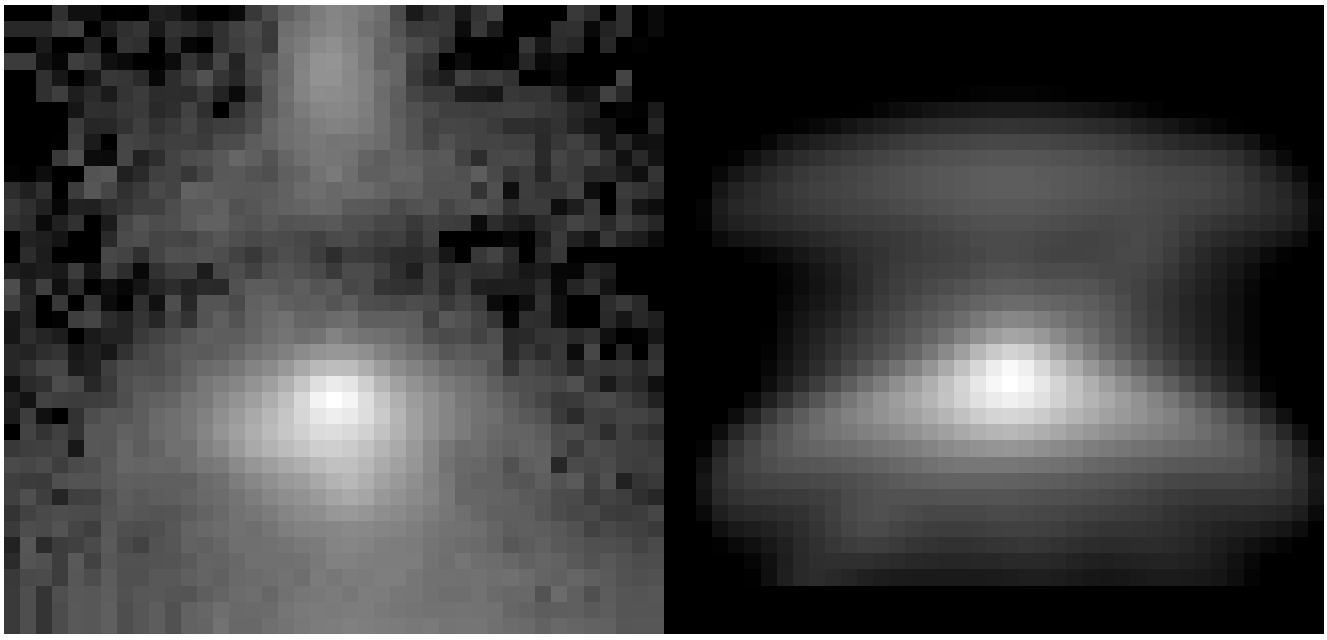

FIG. 6.—*Left:* WFPC2 F675W (*R*-band) image of Haro 6-5B; *right:* single-scattering disk model (PSF convolved) chosen to replicate the width of the obscuration lane and the curvature of the top and bottom surfaces of the disk. Images are logarithmically stretched.

ing software, we hoped for similar success by fitting H6-5B. However, these images have a significantly lower signal-to-noise ratio (on the order of 1 for the fainter, southwest side of the disk) than those used for the HH 30 study, and the fitting software was unable to produce reasonable results.

A further complication in modeling the H6-5B disk is that it is probably more massive and denser than that of HH 30. The 1300 μm H6-5B flux from Reipurth et al. (1993) of 141 $\pm$ 13 mJy is 4 times greater than that of HH 30 (35 mJy), which is presumably indicative of a larger disk mass. For a dust emissivity $\kappa = 0.02$ cm^2 g^{-1} and disk temperature of 40 K, the millimeter flux suggests a disk mass of 0.01 $M_\odot$. More detailed modeling by Dutrey et al. (1996) suggests a somewhat larger mass of 0.04 $M_\odot$. The thicker obscuration lane also indicates a larger mass.

Nevertheless, we can demonstrate the general applicability of disk models to the compact bipolar nebula associated with H6-5B. We calculated a model scattering nebulosity for a disk of appropriate radius. This is shown for comparison with the data in Figure 6. A total disk mass of 0.01 $M_\odot$ (suggested by the millimeter continuum flux) was used, an observer latitude of 13° was selected from the ratio of jet radial velocity to proper motion, and a flaring function less steep than that found for HH 30 was used. The model shows that the star is located at the bright concentration of light seen in the forward-facing side of the disk. No attempt was made to fit the image to optimize the values of these parameters. This shows that a disklike structure can generally reproduce the observed morphology.

4. DISCUSSION

4.1. *FS Taurus A*

FS Tau A is an example of one of the increasing number of recently discovered pre–main sequence binaries. The fluxes of FS Tau E, which is the fainter component, are well matched by a blackbody with a temperature of 3360 K and an extinction of $A_V = 8.1$ ($A_K = 0.75$). The derived luminosity of 0.8 $L_\odot$ corresponds to a 0.2 $M_\odot$ star of age 10^5 yr, according to the evolutionary tracks of D'Antona & Mazzitelli (1994).

No reddened blackbody energy distribution appears to match the fluxes for FS Tau W. If we constrain the curve to fit our V and I photometry, the K-band brightness is over 2 mag fainter than that observed (9.8 predicted vs. 7.4 observed). This is true over a reasonable range of blackbody temperatures (2500–4700 K) and extinctions. We are confident of our optical photometry, since the combined values agree with those observed from the ground. A K-band excess from hot dust at a few stellar radii could account for this discrepancy. However, the 2 mag required is greater than the largest K excess derived for a sample of 36 classical T Tauri stars by Strom et al. (1989). The apparent K excess for FS Tau W is either very large or an artifact of significant source variability.

As mentioned previously, the binary fluxes for a number of stars derived from lunar occultations by Simon et al. (1992) tend to agree with the speckle measurements of Ghez et al. (1993), even though the orientations of some of the pairs differ by tens of degrees. The lunar occultation values are the only infrared fluxes available for each component of FS Tau.

There are some discrepancies among the observed K-band fluxes. The combined photometry from Simon et al. (1992) is $K = 7.3$. VRZ85 measured $K = 8.03$ in a 15″ diameter aperture, and Tamura & Sato (1989) obtained $K = 7.9$ in a 36″ diameter aperture (which should still exclude H6-5B). The latter two measures likely included some scattered light from the surrounding nebulosity and so overestimated the combined stellar flux. The differences between the combined value from Simon et al. (1992) and the aperture fluxes are within the range of K-band variations seen in T Tauri stars. Better measurements of FS Tau A in the infrared are required, perhaps using speckle L-band interferometry.

Previous studies have developed a circumstellar disk interpretation for the nebulosity surrounding the FS Tau binary. The significant polarization of the direct starlight (GS89), combined with the *IRAS* excesses assigned to FS Tau, was the basis for this model. Our *HST* images show no clear evidence for a disk around the binary, at least on scales greater than about 60 AU. The reflected light at a 500 AU scale is elongated at P.A. = 132°. In a simple, single scattering nebula, a net polarization angle perpendicular to the long axis of this nebula (or 52°) would be expected. Instead, the measured polarization direction is near 84° over the wavelength range 0.7–2.0 μm, while the polarization magnitude drops from 10% to 1%–2% (GS89; Whitney, Kenyon, & Gomez 1997; Tamura & Sato 1989). The misalignment of the net polarization vector with the larger nebula, combined with the relatively constant position angle of the polarization with wavelength, suggests that transmission through aligned dust grains might be the dominant polarization mechanism. In that case, the close agreement in the position angles of the polarization and binary separation vectors could be explained by aligned grains in a dipole magnetic field whose axis was perpendicular to the binary separation. However, the decreasing magnitude of the polarization with wavelength is more consistent with the expected decreasing contribution of reflected light at longer wavelengths as the dust scattering efficiency decreases. The scale of that nebulosity would have to be restricted to within 50 AU of the binary to escape detection with WFPC2.

The spectral energy distribution of FS Tau A has also been used to argue for the presence of a circumstellar disk. FS Tau and H6-5B are spatially confused in the *IRAS* beams, and the combined source is known as IRAS 04189+2650. Kuiper Airborne Observatory measurements at 47 and 95 μm by Cohen, Harvey, & Schwartz (1985) also employed large beam sizes that could not separate the contribution of each source. Cohen & Schwartz (1987) apportioned the *IRAS* fluxes according to the relative brightness of each source at 3.5 μm, which assigns 95% of the flux to FS Tau A. Adams, Emerson, & Fuller (1990) assumed that all of the IRAS 04189+2650 fluxes belong to FS Tau A and presented a disk model for the resulting infrared spectrum. However, there are strong reasons to believe that H6-5B is actually the brighter infrared source. Millimeter continuum measurements now indicate a much larger circumstellar mass for the jet source than for the binary (Reipurth et al. 1993; Beckwith et al. 1990). We will show that the jet source is much more obscured than the binary ($A_V = 23$ vs. $A_V = 8$), and this will significantly affect any division of the *IRAS* fluxes based on near-IR measurements. Finally, we actually observe the disk as the dust lane in H6-5B. It seems probable that H6-5B is the largest contributor to the fluxes of IRAS 04189+2650.

4.2. *Haro 6-5B*

There are a number of explanations for the large hourglass structure centered on H6-5B. As suggested by EM98, it could represent the edges of a bipolar cavity that has been cleared by winds from H6-5B. The star would illuminate the cavity's surface, creating a limb-brightened hourglass. Structures of this type are seen around a number of young stellar objects (L1551 IRS 5, for instance). The northeast/southwest symmetry seen in the hourglass would arise from symmetrical winds. However, the northeast lobe is filled with dark nebulosity and the southwest lobe contains the R2 nebula, so it is unlikely that these are cleared regions.

Rather than the hourglass being a physical structure, we favor a model in which it is caused by a bipolar light cone defined by the H6-5B disk that illuminates the nebulosity in the region. This would explain why the R1 and R2 nebulae do not appear to extend beyond the hourglass. The interior of the southwest lobe is not fully illuminated, however. This may indicate that either some dark nebulosity is responsible for shadowing or that the brighter regions are due to higher nebula densities. The R2 nebula may even cause shadowing. There is a star located in the brighter part of the lobe that may also contribute to the local intensity increase.

In this scenario, the nebula R1 is the illuminated portion of the dark nebula that fills the northeast lobe. As shown schematically in Figure 7, the surface of the nebula near H6-5B may resemble an inclined plane, so that the intersection of the light cone with the plane would form a parabolic shape like that seen. The $I-R$ image in Figure 5 shows that the edge of R1 is redder than the interior. This may be due to reddening of light by dust in the disk toward the outer limit of the cone. The dark lane separating R1 from H6-5B would be the portion of the plane projecting behind H6-5B that is not illuminated by the light cone rather than obscuration by dust between the two objects. The dark nebula would shadow itself, with the jet passing through it and reappearing later. If the above interpretation is correct, then the opening angle of the hourglass would provide a constraint on disk models.

This scheme is similar to that proposed by GS89. However, they were unaware of the extent of the southwest lobe and of the dark nebula filling the northeast lobe. Their polarization measurements indicated that the source of illumination for the biconical structure, which they called H6-5C, was located in the R1 nebula. However, we see no evidence for any such source within R1, and H6-5B is clearly at the center of the hourglass. R1 is likely to remain fairly bright in the near-infrared owing to scattered light, which may account for the IR position offset from H6-5B as measured by VRZ85.

EM98 assumed that the hourglass was a cleared cavity based on its resemblance to other objects and line emission seen in the structure, presumably owing to interactions with the surrounding medium. Most of the line emission might be explained by reflection of light from the H6-5B source

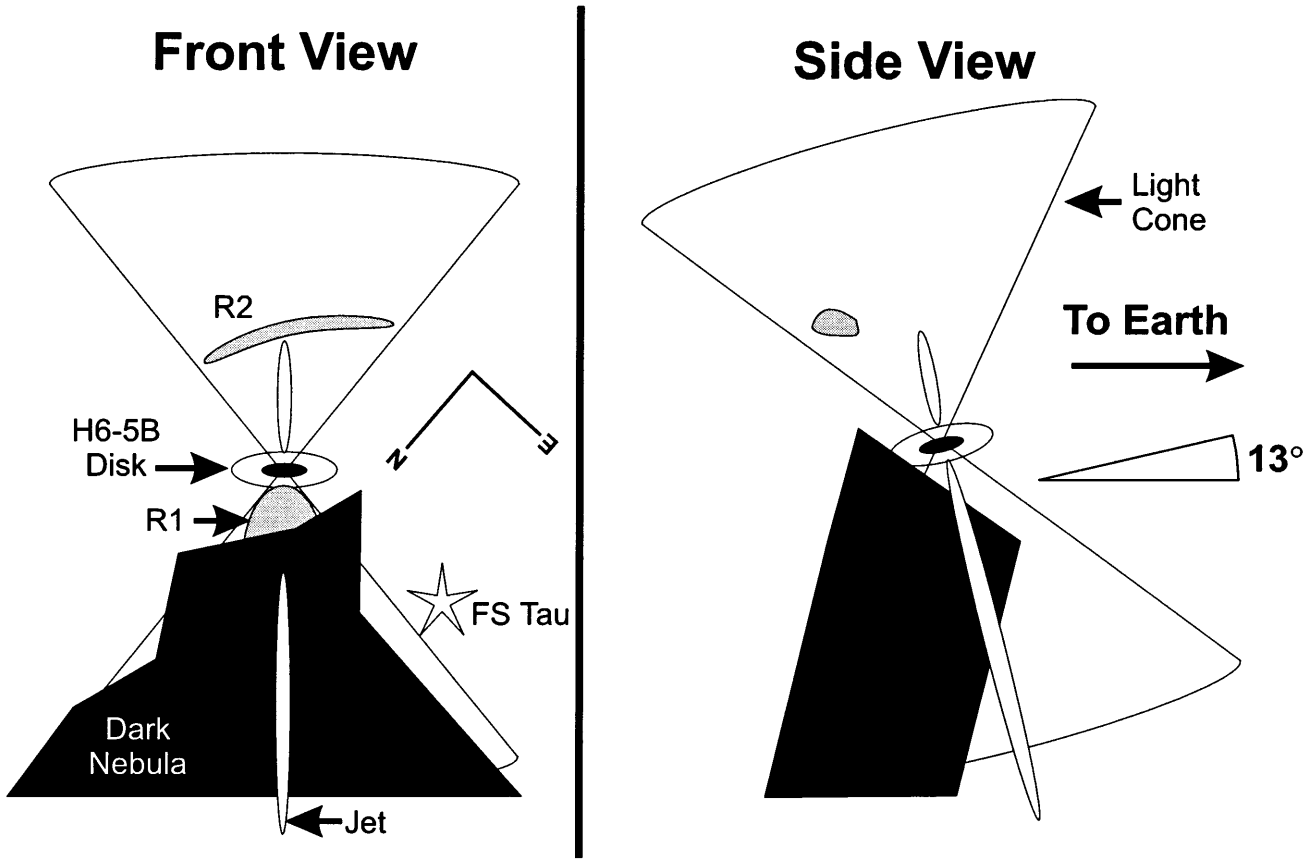

FIG. 7.—Schematic of a possible distribution of light and nebulae that could produce the observed images of the FS Tauri field. A bipolar cone of light is formed by the Haro 6-5B disk that illuminates the surrounding nebulosity. The intersection of the cone and the dark nebula creates the bright, conical nebula R1 and the arc-shaped nebula R2. The jet passes through the dark nebula, which creates its own shadow.

and jet. H6-5B has an Hα emission line like other young, T Tauri stars, as was detected in the spectra of the R1 nebula. In the Hα-I image of EM98, the interior of the northeast lobe appears to be filled with faint nebulosity, which might be explained as Hα emission from the jet being reflected by the dark nebula behind it. There are two knots of line emission (c_1 and c_2) seen in the EM98 images along the southern edge of the southwest lobe that do not appear in either our or their *I*-band frames that we cannot explain (they are outside of the field of our *R*-band image).

The northeast jet appears to show both long and short-period oscillation patterns at distances of 24″–40″ from H6-5B. The long-period pattern, which resembles that seen in the jet of HH 30, has an approximate transverse amplitude of 1″ and a wavelength of 24″, of which about one-half of a period is seen. This may indicate that the source is precessing. Assuming a jet proper motion of 150 km s^{-1}, the precession period would be approximately 100 yr. The short-period pattern has an amplitude of 0.″4 and a wavelength of 2.″5, which implies an oscillation period of 10 yr. The cause of these flow oscillations is not known. They could be intrinsic to the jet source (precession) or propagation effects as the jet passed through the dark cloud.

MRR91 present measurements for the width of the H6-5B jet made in 1″ seeing that lead to the conclusion that the jet width narrows by a factor of 2 over the distance range of 17″–40″ from the source. de Gouveia dal Pino, Birkenshaw, & Benz (1996) have calculated three-dimensional numerical simulations of protostellar jets propagating into density-stratified ambient media. Their models yield converging jets in the case of an ambient medium whose density increases with distance, and they cite H6-5B as an example in which this phenomenon is observed. However, our images show that the large jet width obtained by ground-based observations actually reflects the amplitude of the short-period "wiggles." Variation in the amplitude of the wiggles may be the most important factor in defining the jet width as measured with 1″ resolution. Since the situation is clearly more complex than the converging axisymmetric jet previously considered, it is not clear that the structure of the H6-5B jet is a good match to Figure 1*a* of de Gouveia dal Pino et al. (1996).

As previously discussed, we were unable to produce a detailed model for the H6-5B disk. However, we can make some general assumptions about the disk. Based on our early modeling of HH 30 (Burrows et al. 1996), it is apparent that the H6-5B disk is inclined by 10°–18°. The fact that both sides of the disk are concave and parallel to each other indicate that its inclination is greater than that of HH 30 ($<7°$) but not so much as to cause light scattered from the rearward-facing side to be blocked by the disk itself. Also, if we assume a maximum jet velocity of 300 km s^{-1}, then the observed jet radial velocity of $\sim$70 km s^{-1} would imply an inclination of about 13°.

The disk H6-5B appears thicker and flatter than the HH 30 disk. The larger obscuration lane that divides the illuminated sides is indicative of a disk mass that is greater than that of HH 30. This agrees with the larger millimeter flux, as mentioned previously.

The bright concentration of light in the disk is probably at the location of the star. The greater inclination of the disk (compared to HH 30) reduces the line-of-sight extinction toward the source. In HH 30, the extinction was so great owing to the edge-on orientation that there was no indication of the star's location at visual wavelengths. Recent 2 μm observations (Stapelfeldt et al. 1998c) have shown that the HH 30 source is still obscured at that wavelength. In comparison, the H6-5B source should be more apparent in the infrared. If the extinction of the star along the line of sight were known, it would provide a strong constraint on future models. However, as with HH 30, we currently can derive only a crude estimate from the near-infrared fluxes. The median *K* magnitude for a T Tauri star in the Taurus-Auriga region is $K < 9$ (Kenyon & Hartmann 1995; Strom et al. 1989). H6-5B has a *K* magnitude of 11.55 ± 0.05 (VRZ85). If we assume that the star has an unreddened magnitude of $K = 9$, so that $A_K = 2.6$, then the extinction based on standard interstellar grain properties would be $A_I \sim 18$ and $A_V \sim 23$. For comparison, HH 30 has a *K* magnitude of 13.16 ± 0.12 (VRZ85). Therefore, we assume that $A_I \sim 18$ is a lower extinction bound. Upcoming *HST* near-infrared camera and multiobject spectrometer (NICMOS) observations should provide an accurate value for extinction if the source is visible in the near-infrared (D. Padgett 1998, private communication).

Future modeling efforts should take into account that the disk mass being greater than that of HH 30 implies a larger midplane extinction, so that even at infrared wavelengths the disk is not optically thin. Thus, material in the midplane may be colder and more dense than implied by a simple dust distribution model that matches the visible portion of the disk.

5. CONCLUSIONS

HST observations of the field of FS Tauri reveal a complex pattern of reflection nebulosity surrounding the binary star FS Tauri A and the nearby Haro 6-5B. The *HST* images clearly resolve for the first time at visual wavelengths the two components of FS Tau A that have a separation of 0.″24. The eastern, fainter component is well matched to a 3360 K blackbody with an extinction of $A_V \sim 8$. The brighter component is not well matched by any reasonable blackbody with extinction, having a 2 mag brightness excess at *K*. The binary is surrounded by a complex, filamentary nebula that is a few arcseconds long and oriented at P.A. = 132°. There is no sign of a circumstellar disk, which was favored in previous studies based on polarization and wide-field infrared measurements.

The nearby young star, Haro 6-5B, is surrounded by a compact reflection nebula, divided by a lane of obscuration. It appears to be a protostellar disk like that of HH 30. Scattering by the disk prevents direct detection of the star at visual wavelengths. A bipolar jet is seen extending from the disk. Toward the northeast the jet is twisted, which explains the unusual width measurements obtained by ground-based observers. A large, hourglass-shaped pattern of reflection nebulosity is seen aligned along the jet axis and centered on H6-5B. This is presumably the intersection of the surrounding nebulosity with the cone of light from the clear polar regions of the H6-5B disk. The interior of the northeast lobe of the hourglass appears to be filled by a dark nebula that is illuminated along its southern edge by FS Tau A.

This work was supported by the WFPC2 Investigation Definition Team under a grant from the National Aeronautics and Space Administration. The authors thank the referee, M. Simon, for his useful comments.

REFERENCES

Adams, F. C., Emerson, J. P., & Fuller, G. A. 1990, ApJ, 357, 606
Beckwith, S. V. W., Sargent, A. I., Chini, R. S., & Gusten, R. 1990, AJ, 99, 924
Burrows, C. J., et al. 1996, ApJ, 473, 437
———. 1998, in preparation
Chen, W. P., Simon, M., Longmore, A. J., Howell, R. R., & Benson, J. A. 1990, ApJ, 357, 224
Cohen, M., Harvey, P. M., & Schwartz, R. D. 1985, ApJ, 296, 633
Cohen, M., & Fuller, G. A. 1985, ApJ, 296, 620
Cohen, M., & Kuhi, L. V. 1979, ApJS, 41, 743
Cohen, M., & Schwartz, R. D. 1987, ApJ, 316, 311
D'Antona, F., & Mazzitelli, I. 1994, ApJ, 90, 467
de Gouveia dal Pino, E. M., Birkenshaw, M., & Benz, W. 1996, ApJ, 460, L111
Dutrey, A., Guilloteau, S., Duvert, G., Prato, L., Simon, M., Schuster, K., & Menard, F. 1996, A&A, 309, 493
Eislöffel, J., & Mundt, R. 1998, AJ, in press
Elias, J. H. 1978, ApJ, 224, 857
Ghez, A. M., Neugebauer, G., & Matthews, K. 1993, AJ, 106, 2005
Gledhill, T. M., & Scarrott, S. M. 1989, MNRAS, 236, 139 (GS89)
Gledhill, T. M., Warren-Smith, R. F., & Scarrott, S. M. 1986, MNRAS, 223, 867
Kenyon, S. J., & Hartmann, L. 1995, ApJS, 101, 117
Krist, J. E. 1996, Tiny Tim User's Manual V4.1
Krist, J. E., et al. 1997, ApJ, 481, 447
Mundt, R., Brugel, E. W., & Bührke, T. 1987, ApJ, 319, 275 (MMB87)
Mundt, R., Bührke, T., Fried, J. W., Neckel, T., Sarcander, M., & Stocke, J. 1984, A&A, 140, 17
Mundt, R., Ray, T. P., & Raga, A. C. 1991, A&A, 252, 740
Reipurth, B., Chini, R., Krügel, E., Kreysa, E., & Sievers, A. 1993, A&A, 273, 221
Simon, M., Chen, W. P., Howell, R. R., Benson, J. A., & Slowik, D. 1992, ApJ, 384, 212
Stapelfeldt, K. R., et al. 1995, ApJ, 449, 888
———. 1997, BAAS, 29, 1216
———. 1998a, ApJ, submitted
———. 1998b, in preparation
———. 1998c, in preparation
Strom, K. M., Strom, S. E., Edwards, S., Cabrit, S., & Skrutskie, M. F. 1989, AJ, 97, 1451
Tamura, M., & Sato, S. 1989, AJ, 98, 1368
Vrba, F. J., Rydgren, A. E., & Zak, D. S. 1985, AJ, 90, 2074
Whitney, B. A., Kenyon, S. J., & Gomez, M. 1997, ApJ, 485, 703